Mechanical Engineering Advances 2025, 3(3), 2587.
https://doi.org/10.59400/mea2587

Article

Optimization of mirror mount design based on opto-mechanical performance for space applications

Fatouma Maamar

Algerian Space Agency, Satellites Development Center, USTO, POS 50 ILOT T12 Bir El Djir, ORAN 31130, Algeria; fmaamar@cds.asal.dz

CITATION

Maamar F. Optimization of mirror mount design based on opto-mechanical performance for space applications. Mechanical Engineering Advances. 2025; 3(3): 2587. https://doi.org/10.59400/mea2587

ARTICLE INFO

Received: 14 January 2025
Revised: 8 May 2025
Accepted: 13 May 2025
Available online: 1 July 2025

Abstract: A new fixation type for mirror assembly was proposed in space telescope. The optomechanical design of a large aperture is necessary to maintain the stability of the optical structure regarding environmental disturbances, restrictions on the weight, size and shape of the mirror, which must be satisfied for space applications. This paper presents a study focusing on the optimal optomechanical design for mirror mounting using glue pad bonding. We have developed a new design specifically tailored for the BK-7 mirror with a diameter of 500 mm and a thickness of 45 mm. The primary aim of this research is to determine the optimal combination of glue pad number, size, and thickness to minimize both glue stress and errors in the mirror's shape. To achieve this, we conduct simulations under various load cases, varying the size and thickness of the glue pads. The new design results demonstrate the effectiveness of the proposed optimization method, which greatly minimizes thermal stress in the mirror and ensures adequate supporting stiffness. This solution for the mirror and mount design can provide valuable support to decision-makers and optical engineers during the development phase of space optomechanical systems.

Keywords: optomechanical design; mirror assembly; glue pad bonding; margin of safety (MOS); mirror distortion

1. Introduction

Large mirrors are commonly used in applications such as telescopes and laser optical systems. However, mounting and supporting large mirrors presents greater challenges compared to lenses, as mirrors are significantly more sensitive to distortion. Unlike lenses, which have multiple refractive surfaces, mirrors rely on a single reflective surface, making them more susceptible to errors caused by surface deformations. Achieving high performance in mirror mounting requires an integrated optomechanical analysis to accurately predict mirror behavior. This integration necessitates the precise transfer of finite element analysis (FEA) results into optical analysis programs [1].

Chin [2] introduces the fundamental design objectives for optical mirror mounts. A successful mounting system should minimize optical distortions while allowing for a straightforward alignment process. Additionally, the mount must mitigate thermal and assembly stresses to prevent surface figure distortion while providing sufficient supporting stiffness to resist displacement due to gravity [3–5]. As more advanced techniques for designing space telescope mirrors emerge, early designs have often been based on empirical experience. Over time, optimization approaches such as topology optimization, size optimization, and parametric design have become prevalent in mirror design.

Liu and Jiang conducted a topology optimization study on a lightweight primary mirror for a large telescope, considering constraints such as self-weight and polishing pressure. Their objective was to minimize structural compliance and mass, with the optimized results demonstrating significant improvements in mirror performance [6–10]. Liu [11] further proposed a parametric optimization method based on topology optimization to minimize the root mean square (RMS) of surface accuracy and mirror mass. Jiang [12] applied topology optimization to a silicon carbide (SiC) primary mirror to address axial support position sensitivity. Similarly, Zhang and Chen [13–14] optimized a lightweight Zerodur primary mirror and bipod flexure, successfully reducing the RMS value of surface accuracy.

These studies highlight the effectiveness of optimization in improving mirror surface accuracy (RMS) [15–17]. However, existing research does not extensively cover bonding techniques for mounting mirrors with flexures. The primary challenges in mirror mounting include stress distribution, glass strength, thermo-elastic effects, safety margins, and potential distortions in the mirror. This study examines the material properties of glass, metal, and adhesives used in mirror mounting. In designing glue pads for bonding, factors such as high shear strength and relatively low peel strength in adhesively bonded metal systems must be considered. The number of adhesive contact points also plays a critical role in joint strength. The most effective approach is to select an optimal adhesive pad configuration for attaching the mirror to the bipod flexure while balancing accuracy, manufacturing feasibility, and cost. However, in some cases, achieving an ideal solution may not be feasible due to design constraints.

This paper proposes a novel approach to determining the optimal configuration for attaching the mirror to titanium bipod flexures using glue pads. The optimization process focuses on minimizing glue pad stress, as well as reducing thermal and mechanical stresses in the mirror, with the ultimate goal of achieving an optimal optomechanical design.

2. Materials and methods

2.1. Model mirror assembly description

Techniques for mounting large mirrors using glass-to-metal bonding with adhesives such as epoxy have gained significant popularity, especially for space applications exposed to harsh environmental conditions. The simplest bonded interface occurs at the back surface of a first-surface mirror, as shown in **Figure 1**. In this design, the fine-ground back surface of a 500 mm diameter, 45 mm thick crown glass mirror is bonded to a flat circular pad on a titanium support using epoxy adhesive. The adhesive thickness ranges from 0.8 to 1 mm. The pad area measures 678.58 mm^2, and the mirror has a mass of approximately 24.846 kg.

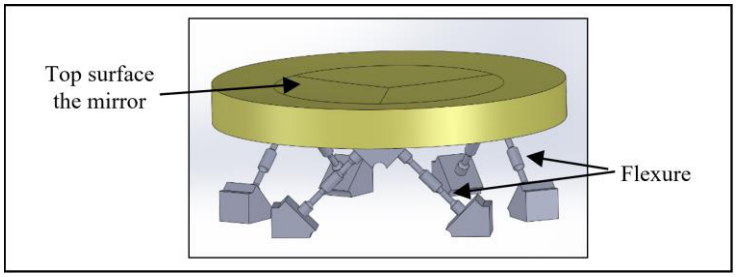

Figure 1. A mirror mounting configuration.

The mirror is subjected to a loading condition where the gravity vector is at an angle to the optical axis, resulting in surface deflections, as illustrated in **Figure 2**. Self-weight deflection of a mirror refers to the displacement caused by the gravitational force acting on the mirror's material mass. There are two primary components of self-weight deflection: axial and radial. Axial deflection, also known as "vertical axis" deflection, occurs when the mirror's optical axis is aligned vertically, representing the worst-case scenario. Radial deflections, on the other hand, occur when gravity acts parallel to the optical surface or perpendicular to the optical axis. This is referred to as "horizontal axis" deflection, which arises when the mirror's optical axis is positioned horizontally relative to the Earth's surface.

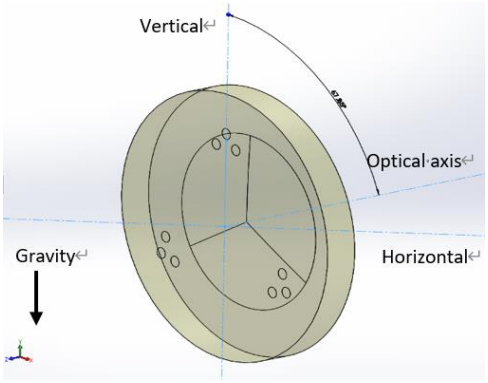

Figure 2. Holding a mirror mounting, defined optical axis.

The mirror is subjected to a loading condition in which the gravity vector is angled relative to the optical axis, resulting in deflections on the mirror surface [18–23]. These deflections lead to:

$$\delta_{\theta-RMS} = \sqrt{(\delta_{A-RMS}cos\theta)^2 + (\delta_{R-RMS}sin\theta)^2} \quad (1)$$

where:

$\delta_{\theta-RMS}$: the mirror RMS self-weight deflection at an angle θ.

δ_{A-RMS}: the mirror RMS self-weight deflection in the axis vertical position.

δ_{R-RMS}: the mirror RMS self-weight deflection in the axis horizontal position.

θ: The angle between the gravity vector and the mirror optical axis.

The self-weight deflection of an axisymmetric concave mirror primarily results in astigmatism, with a change in the optical radius of curvature in the vertical direction, while the horizontal radius remains relatively unchanged.

$$\delta_R = 2C_R \frac{\rho}{E} r^2 \quad (2)$$

where:

δ_R: The self-weight deflection of the mirror in the horizontal position.

C_R: The support parameter.

ρ: The mirror material density.

E: The mirror material elastic modulus.

r: The mirror radius.

The self-weight deflection under axial loading, or along the vertical axis, is estimated using closed-form equations based on classical plate theory. The loading condition assumed for estimating axial plate deflection is a uniform or constant load applied over the plate surface, equivalent to the weight per unit area of the mirror. The axial self-weight deflection for a solid mirror depends on the mirror material, thickness, and internal structure, and is given by:

$$\delta_A = C_A \frac{\rho}{E} (1 - \mho^2) \left(\frac{r}{h}\right)^2 r^2 \quad (3)$$

where:

δ_A: The self-weight deflection of the mirror in the vertical position.

C_A: The support parameter.

ρ: The mirror material density.

E: The mirror material elastic modulus.

$\mho$: The Poisson's ratio of the mirror material.

h: the mirror thickness.

r: The mirror radius.

The radial or axial horizontal deflection is neglected, the mirror self-weight deflection δ_θ at any angle θ between the mirror axis and local vertical is given approximately by:

$$\delta_\theta \approx \delta_A cos(\theta) \quad (4)$$

In this analysis, the assembly is assumed to be approximately thermally stabilized, accounting for both radial and axial deflections of a concave axisymmetric mirror made of BK-7. A three-point axial support is assumed, with the support points spaced equally along 64.5% of the mirror's diameter. Typical calculations show that the deflection of the mirror is 5.19737×10^{-8} m for the support parameter, $C_A = 0.318$.

The models developed in this paper using the finite element method are shown in **Figure 3**, which illustrates various configurations of the contact glue pads. Additionally, **Table 1** presents the precision and tolerance requirements for mirror mounting, specifying the necessary criteria for proper mirror alignment and attachment.

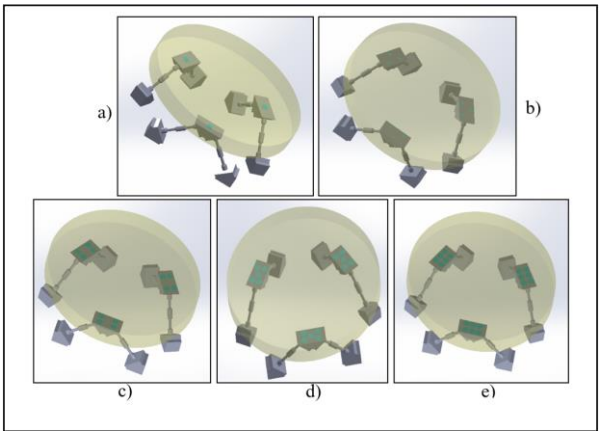

Figure 3. Different attach supports to mirror: **(a)** 1 contact glue pads; **(b)** 3 contacts glue pads; **(c)** 4 contacts glue pads; **(d)** 5 contacts glue pads; **(e)** 6 contacts glue pads.

Table 1. Tolerance guide for mirror [24].

Parameters	**Mirror**
Mirror shape	large
Substrate material	BK-7
Diameter	500 mm
Diameter tolerance	+0.00/−0.20 mm
Angle tolerance	< 3 sec
Radius	250 mm
Thickness	45 mm
Thickness tolerance	±0.03 to ±0.1 mm
Clear aperture	> 95% of diameter
Refractive index at 587.5618 nm wavelength (d-line)	1.5168
Refractive index at 546.0740 nm wavelength (e-line)	1.51872
Abbe number at 587.5618 nm wavelength (d-line)	63.96
Abbe number at 546.0740 nm wavelength (e-line)	64.17
Reflection loss at 587.5618 nm (2 surfaces)	8.1⁒
Optical dispersion (nf-nc)	0.008054
Optical dispersion (nf'-nc')	0.008110
Optimum transmission range	350 nm–2.5 μm
Unparalleled index accuracy	±0.0001 to ±0.0003
Index resolution	± 0.0002 to ±0.0003
Parallelism	2 arc s to 1 arc min
Surface quality	60/40
Bevel	0.1 mm to 0.5 mm

2.2. Model bipod flexure description

A new bipod flexure is employed in many high-precision space mirror mount applications. These flexures are specifically designed to provide moment isolation for the mirror, thereby minimizing surface figure distortion [25–29]. The geometric parametric model of the flexures is shown in **Figure 4**. The structure in position (a) is

parameterized as illustrated in **Figure 4b**. The supports, which vary in thickness, provide compliance for the structure. To ensure proper configuration, the thicknesses of each domain are treated as adjustable variables that can be optimized to enhance the design.

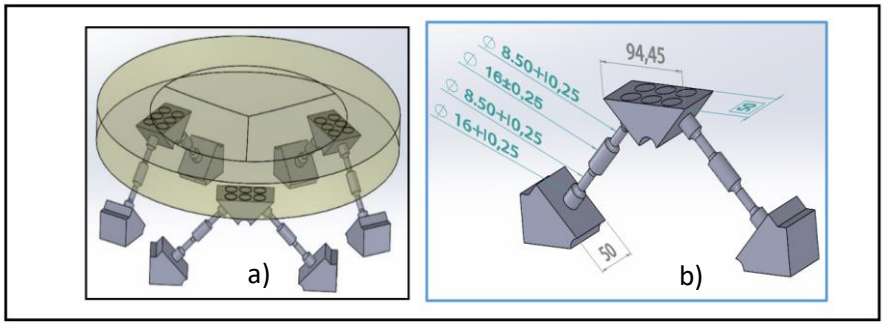

Figure 4. Conceptual configuration of mirror mounting: **(a)** geometry model; **(b)** parametric model of the flexure in mm.

The bipod flexure consists of three identical chains arranged symmetrically in a circumferential pattern. Each chain provides two orthogonal translational constraints: one along the support direction and the other along the tangential direction. To validate the design's effectiveness, an in-depth optimization process was conducted to determine the optimal geometric and size parameters for the flexure. Subsequently, finite element analysis (FEA) simulations of both the flexure and the overall system were performed. The analysis focused on examining how the axial and circumferential positioning of the three flexures affects the mirror's surface figure, with the objective of improving performance after optimization.

2.3. Finite element model analysis

In this section, several models were created using SolidWorks 2020 software to illustrate the various configurations and support the different cases outlined in **Table 2**. The parameters defining the cases configuration of the glue pads are based on the heritage of the optomechanical design of large apertures, ensuring the stability of the optical structure. Additionally, the size and shape constraints of the mirror, which must be met for space applications. The mechanical and thermal properties of the materials used in these models are presented in **Table 3**, with references to sources [30–32]. These properties are crucial for understanding the behavior and performance of the materials under the specified conditions.

Table 2. Parameters defining the cases configuration of the glue pad.

Cases Study
Case 1: 1 contact, 40mm diameter, 1mm thickness
Case 2: 1 contact, 40mm diameter, 0.8mm thickness
Case 3: 1 contact, 20mm diameter, 0.8mm thickness
Case 4: 3 contact, 20mm diameter, 0.8mm thickness
Case 5: 3 contact, 10mm diameter, 0.8mm thickness
Case 6: 4 contact, 20mm diameter, 0.8mm thickness
Case 7: 5 contact, 20mm diameter, 0.8mm thickness
Case 8: 6 contact, 20mm diameter, 0.8mm thickness

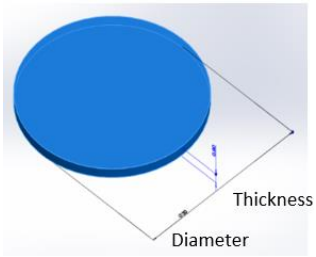

Table 3. Parameters defining the materials.

Part	**Support**	**Glue**	**Mirror**
Material	Titanium	Epoxy	BK 7
Young's Modulus E(MPa)	$1.13x10^5$	(4700/70) for (−40 °C/20°C) [33]	82,000
Poisson's Ratio ν	0.32	0.39	0.257
Coefficient of Thermal Expansion CTE.10^{-6} (/K)	7	102	0.21
Mass Density ρ (kg/m^3)	4501	1260	2520

The mesh model of the mirror assembly was created using Ansys 2020 R2 software, as shown in **Figure 5**. To accurately analyze the thermo-elastic stress at the glue pads, it was determined that a finer mesh is necessary. This refined mesh uses linear quadrilateral and quadratic quadrilateral elements, as shown in **Figure 6**, to ensure a precise analysis of the stress distribution.

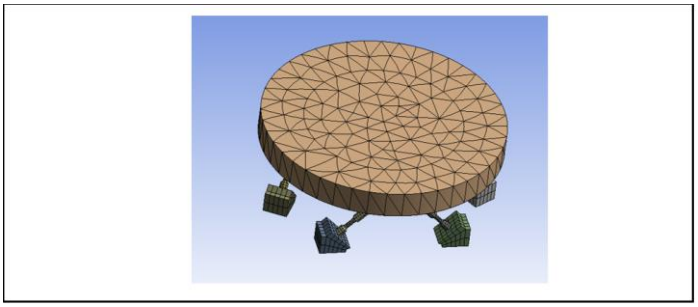

Figure 5. Default mesh for assembly monitoring.

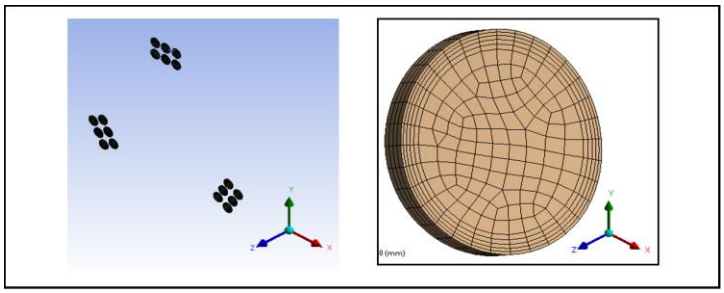

Figure 6. Refined mesh for glue pad (Exp; 6 contacts number).

The base of the main housing stand is fixed, providing six degrees of freedom (DOF) for the elements used. The DOFs for solids include translations along the *x*, *y*, and *z* axes. The mirror assembly is analyzed under the following load conditions, as illustrated in **Figures 1**, **7**, and **8**, which show the boundary conditions applied to the different models:

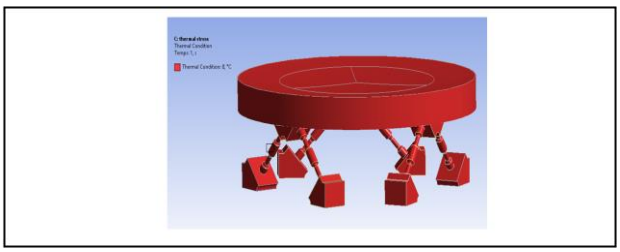

Figure 7. Thermal load distribution at 20 ℃ for assembly monitoring.

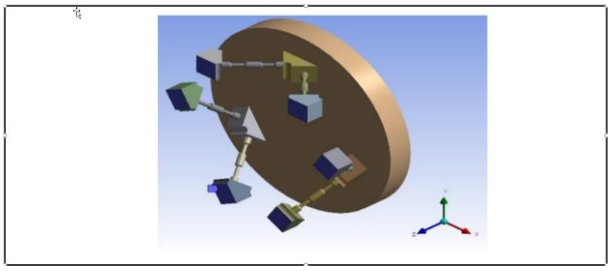

Figure 8. Fixed supports for assembly monitoring.

- Ambient temperature: T = +20 ℃
- Thermal load: The structure is subjected to temperature variations of 0 ℃, −10 ℃, −20 ℃, and −30 ℃.
- Inertial loads: A 1 g inertia force is applied in the *X*, *Y*, and *Z* directions.
- Top surface: The top surface is free to move in all directions, as shown in **Figure 1**.
- Bottom boundary of the flexures: The bottom boundary of the flexures is fixed in all directions, as shown in **Figure 8**.

3. Results and discussions

In this section, several simulations were conducted using various approaches, all aimed at converging towards the optimal configuration, which is defined as follows:

3.1. Thermoelastic analysis

In this sub-section, thermo-elastic stress analyses were performed to determine the stress on the glue pads resulting from thermal loads. Thermal loads are defined as the internal stresses in a structure caused by expansion (due to the coefficient of thermal expansion, CTE) when exposed to a temperature field that deviates from the stress-free condition. Thermo-elastic stresses were calculated for four temperature conditions: 0 ℃, −10 ℃, −20 ℃, and −30 ℃, which cover all expected non-operating testing conditions for the assembly.

Table 4 presents the maximum thermo-elastic stresses for each glue pad element, in MPa, corresponding to different temperatures and cases.

Table 4. The thermo-elastic stresses for each element "glue pads" in MPa for different temperatures and different cases.

Cases	Temperature (℃)			
	0 ℃	**−10 ℃**	**−20 ℃**	**−30 ℃**
Case 1	3.6107	8.7586	15.169	23.199
Case 2	3.6003	8.7281	15.097	23.064
Case 3	4.0348	9.0218	15.482	23.554
Case 4	3.6451	8.8697	15.338	23.421
Case 5	3.8505	9.0153	15.525	23.652
Case 6	3.641	8.9706	15.491	23.634
Case 7	3.6713	9.0006	15.531	23.626
Case 8	3.5926	8.9627	15.480	23.679

From **Table 4** and **Figure 9**, it can be concluded that the results demonstrate a direct proportionality between stress and the stiffness of the optomechanical system. A reduction in the number of glue pad contacts leads to an increase in stress, as outlined in the following points:

- The highest stress occurs in case 8, which involves six contact glue pads between the mirror and support at a temperature of −30 ℃.
- Stress increases from 0 ℃ to −30 ℃, regardless of the number of glue pad contacts across all eight cases.
- The lowest stress is observed in case 8, with six contact points using 20 mm diameter and 0.8 mm thickness glue pads between the support flexure and mirror.

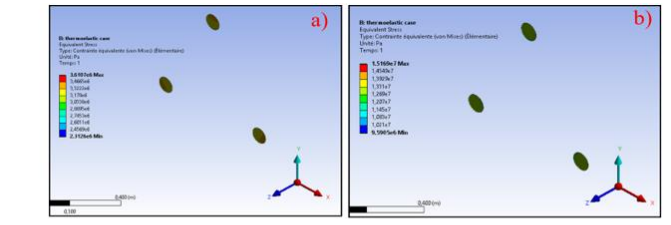

Case 1: Parametric glue pad; 1 contact, 40 mm diameter, 1 mm thickness

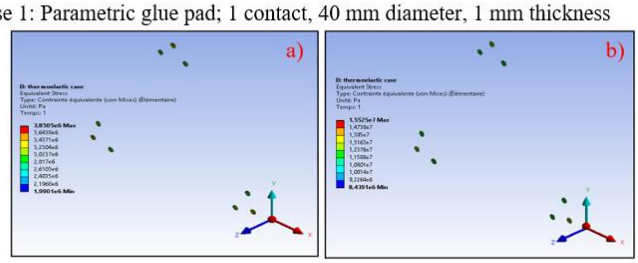

Case 5: Parametric glue pad; 3 contacts, 10 mm diameter, 0.8 mm thickness

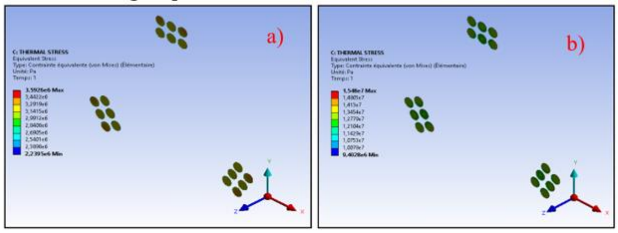

Case 8: Parametric glue pad; 6 contacts, 20 mm diameter, 0.8 mm thickness

Figure 9. Equivalent Von-Mises stress distribution for 03 cases at: **(a)** 0 ℃, **(b)** −20 ℃.

Figures 10–13 illustrate the distribution of maximum stress versus temperature based on the number of glue pad contacts for mirror and bipod flexure. From these figures, we observe that stress increases as the temperature decreases, regardless of whether the element is the mirror or the support flexure. The results indicate that, over a wide temperature range, the material properties of the glue pads exhibit non-linear behavior. These non-linear properties impact the Von-Mises stresses, as the material properties change independently between ambient and operating temperatures.

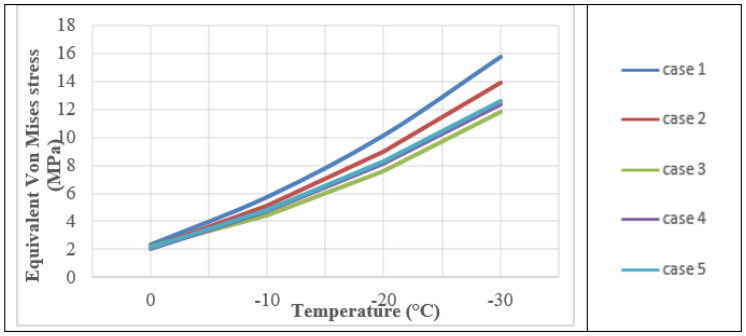

Figure 10. Equivalent Von-Mises stress curve as a function of the temperature for cases 1 through 5 regarding mirror.

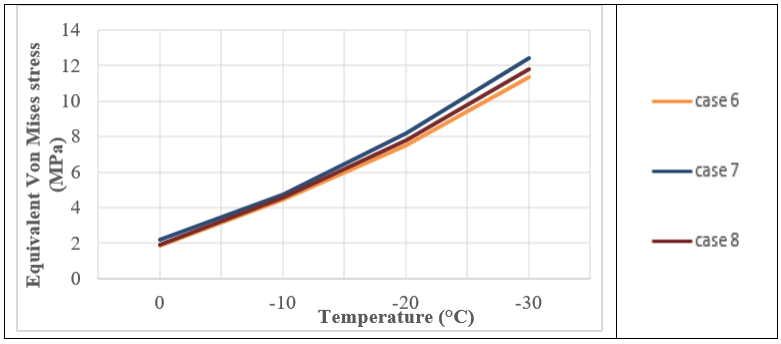

Figure 11. Equivalent Von-Mises stress curve as a function of the temperature for cases 6 through 8 regarding mirror.

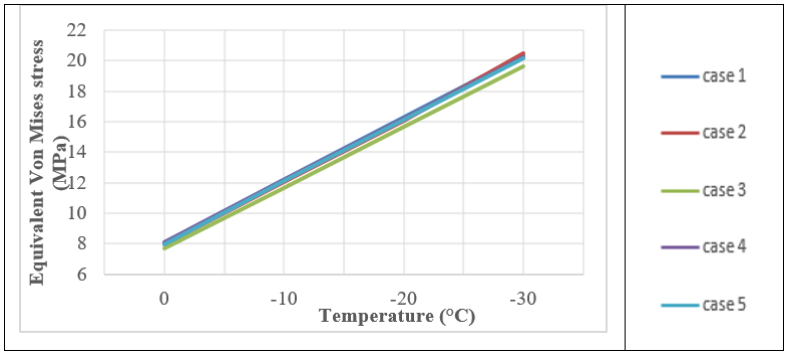

Figure 12. Equivalent Von-Mises stress curve as a function of the temperature for cases 1 through 5 regarding bipod flexure.

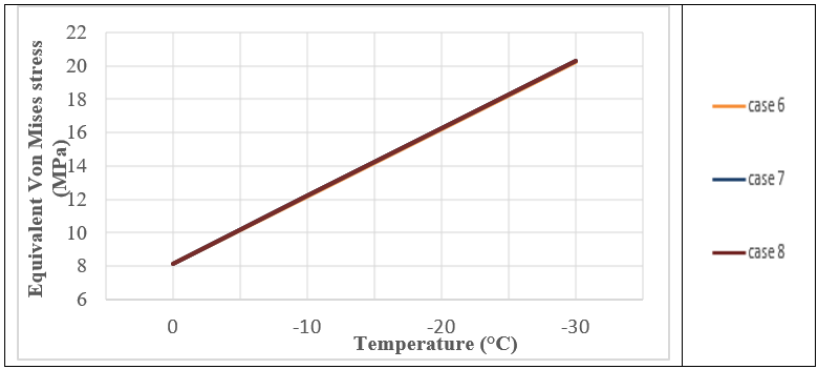

Figure 13. Equivalent Von-Mises stress curve as a function of the temperature for cases 6 through 8 regarding bipod flexure.

Figure 14 displays the Von-Mises stress distribution for 1, 3, and 6 glue pad contacts at temperatures of 0 °C and −20 °C for the mirror. Similarly, **Figure 15** shows the Von-Mises stress distribution for the same number of glue pad contacts at 0 °C and −20 °C for the support flexure. The bonding assembly ensures the attachment and alignment of the optical elements while generating low stress at the contact surface. However, the glue pad must be carefully selected to minimize stress, outgassing, and the risk of disassembly. Optimizing performance requires careful adjustments, and constraints alone are insufficient for performing thermo-elastic linear analyses. Therefore, an alternative analytical approach is employed to determine the optimal number of contact glue pads between the mirror and the assembly, with minimal constraints, using the margin of safety coefficient.

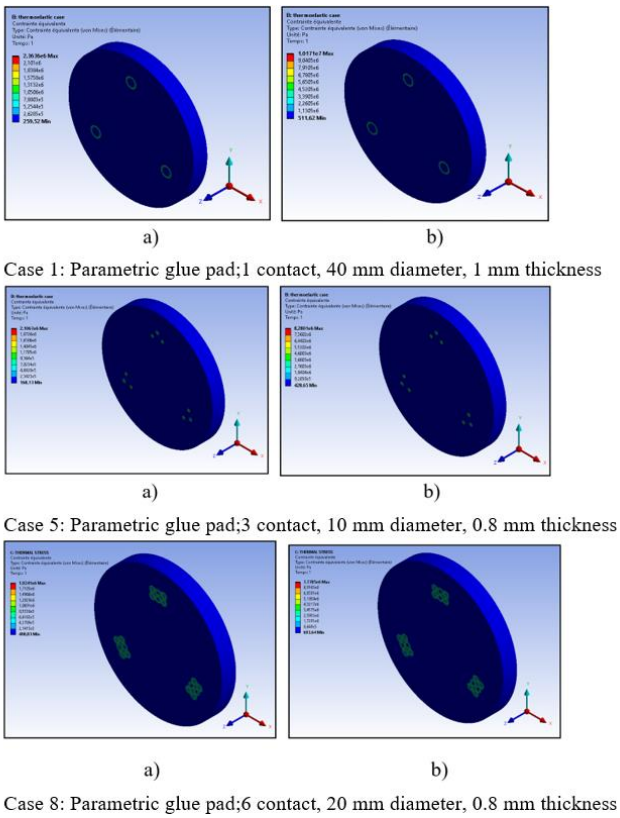

Figure 14. Equivalent Von-Mises stress distribution for mirror at: **(a)** 0 °C; **(b)** −20 °C.

From **Figures 10** and **13**, we observe that the distribution of Von-Mises stresses, particularly near the adhesive contact zone in configurations with 1, 3, 4, 5, and 6 adhesive contacts, is significant in the mirror relative to the support flexure. The stress distribution in the mirror is notably higher near the contact zone with the flexure-adhesive-mirror, where it is influenced by loading and boundary conditions. **Figures 14** and **15** also highlight the non-symmetry in the Von-Mises stress distribution due to varying loading and boundary conditions.

Isothermal loads result in the lowest stresses, with stress differences remaining minimal at a maximum of 1 MPa regardless of the number of contact points, size, or thickness of the glue between the support flexure and the mirror. However, as the number of contacts increases, stress is reduced, particularly when smaller sizes are used compared to other configurations.

After considering the primary thermal load, which aims to minimize stress, the results show that two cases: case 2 and case 8 provide comparable stress values of 3.6003 MPa and 3.5926 MPa, respectively. However, the second load scenario proved more successful, as it complemented our choice by incorporating the Margin of Safety analysis to assess the likelihood of failure or breakage. The MOS analysis confirmed the stability and reliability of the design under the applied loads, ensuring the optimal configuration for the mirror assembly.

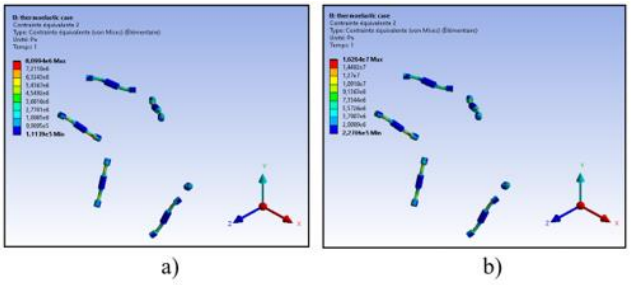

a) b)

Case 1: Parametric glue pad;1 contact, 40 mm diameter, 1 mm thickness

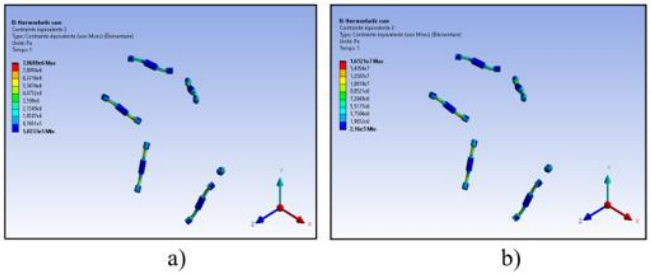

a) b)

Case 5: Parametric glue pad; 3 contact, 10 mm diameter, 0.8 mm thickness

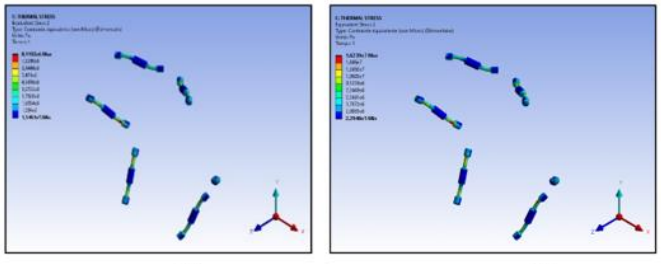

a) b)

Case 8: Parametric glue pad; 6 contact, 20 mm diameter, 0.8 mm thickness

Figure 15. Equivalent Von-Mises stress distribution for bipod flexure at: **(a)** 0 ℃; **(b)** −20 ℃.

3.2. Margin of safety

In space structures, margin assessments are performed usually for strength, and stiffness using numerical analyses. In space structures, margin assessments are typically performed for strength and stiffness using numerical analyses, such as the finite element method. In addition, to minimize and optimally select the number of glue pad contacts, a straightforward methodology has been applied to calculate the Margin of Safety for the adhesive under a 1 g static inertial load, considering isotropic (metallic) materials. The safety margin is a relative measure of the material's allowable capacity compared to the maximum working condition, as defined by the procuring activity [32–34].

The basic equation for defining the margin of safety for uniaxial stress is given by:

$$Margin\ Of\ Safety = \left[\frac{Allowable\ load}{safety\ factor \times working\ load}\right] - 1 \quad (5)$$

This equation helps determine whether the material can withstand the applied loads while maintaining a sufficient safety margin to prevent failure. For the optomechanical assembly, the adhesive Scotch Weld has a Factor of Safety (FOS) of 2, and the corresponding allowable load is 9 MPa. The quasi-static effects during the launch environment are considered, with 8 g (i.e., 8 times the gravitational acceleration) for the axial direction and 5 g for the lateral directions. The axial and lateral directions correspond to the *Z*-axis and the *X*, *Y*-axes, respectively. The working load is defined as 3 × Equivalent Von-Mises stress × directional inertial load. **Table 5** Gives the values of the MOS for different cases in three directions.

Table 5. The values of the MOS for different cases in three directions.

Cases	**Margin of Safety**		
	***Z* direction**	***Y* direction**	***X* direction**
Case 1	2.9295	0.1027	−0.0183
Case 2	2.8994	0.0812	−0.0398
Case 3	0.0055	−0.6573	−0.6815
Case 4	0.9568	−0.0155	−0.1279
Case 5	−0.4667	−0.7348	−0.7603
Case 6	2.9816	0.3522	0.2285
Case 7	2.8668	0.2353	0.4622
Case 8	4.7081	0.8717	0.6842

- The Margin of Safety for the analysis is determined by the lowest margin across all cases.
- Failure is predicted when the MOS falls below 0 (minus data), which occurs in cases 1, 2, 3, 4, and 5 with different contact glue pads.
- The MOS values in the *z*-direction for cases 6, 7, and 8, where the geometric parameters (diameter and thickness) of the glue pads are the same but the number of contacts differs, are lower than the allowable load value, providing satisfactory results.

- This analysis aims to minimize the number of glue pad contacts required for attaching the mirror and supports, while ensuring performance and safety.

Ultimately, using three cases with different numbers of contact glue pads, all having the same diameter and thickness, yields better outcomes than using eight cases. However, this study suggests the need for further analysis, particularly focusing on mirror deformation and distortion, to finalize the choice and ensure the optimal design.

3.3. Mirror distortion analysis

In the space industry, one of the most critical components of a satellite, particularly for imaging, is the mirror. Mirrors play a vital role in imaging by facilitating the proper reflection and alignment of the satellite's optical system, especially in terms of handling left and right directional orientations. A key aspect of mirror production is quality inspection. The quality of a mirror is typically assessed based on three parameters: The radius of curvature, reflection, and distortion.

To evaluate distortion or deformation, a standard methodology is employed, which involves calculating the power residual using two key factors: The Peak to Valley (PV) value and the Root Mean Square (RMS) value. These parameters provide a quantitative measure of the mirror's surface accuracy and its overall performance in imaging applications.

The proposed method is based on the concepts outlined in the work of Michels and Genberg [35], where thermal and structural results from Finite Element Analysis (FEA) in Ansys software are converted for further optical analysis. The residuals, represented by the Root Mean Square (RMS) and Peak to Valley (PV) values, are calculated after removing all terms, indicating how accurately the selected set of Zernike polynomials represent the deformation. This data is organized in tabular form and stored in files for the specific optical analysis program, allowing the extraction of power values.

Figure 16 illustrates the created surface for each mirror, named accordingly. The analysis is conducted using SigFit software, where the displacement command is executed on the analysis files. The RMS and PV values (both maximum and minimum) of surface deformation are then calculated on the residual surface after subtracting each polynomial term. A detailed summary of the analysis procedure is provided in **Table 6**.

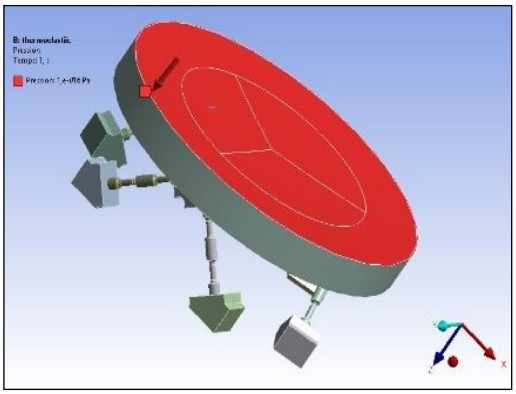

Figure 16. Created named surface for mirror.

Table 6. Values of the RMS (nm) and PV (nm) for three cases.

	Input (Wrt Zero)		**Power (defocus)**		**Pri trfoil**	
	RMS	**PV**	**RMS**	**PV**	**RMS**	**PV**
Case 6	542.1975	1961.3218	6.8518	31.0294	6.4184	24.7883
Case 7	540.6318	1861.7387	7.4395	44.1182	6.1735	25.4555
Case 8	542.0152	1863.5252	7.1497	33.1260	6.3241	26.1458

The residual RMS and PV values consistently decrease as each polynomial term is subtracted. Based on the results, the lowest residual RMS surface deformation occurs in case 8, with 6 contact glue pads entering the mirror and supports, yielding a value of 6.3241 nm. The highest PV value for surface deformation was found to be 26.1458 nm. SigFit software helps identify the best-corrected surface RMS and PV values within the allowable actuator limits. However, to achieve the optimal balance between minimizing glue stress and reducing mirror distortion, the ideal configuration is found to be six (6) glue pad contacts, as seen in case 8. This configuration minimizes the total surface RMS, providing the most effective balance between performance and reliability.

4. Conclusion

This paper presents an optimization process for mirror assembly, focusing on the optomechanical design for space applications. The proposed method integrates computer-aided drafting, finite element analysis (FEA), and an optimization solver to achieve optimal results. FEA was utilized to evaluate thermo-elastic stress, margin of safety, and mirror surface deformation key factors in ensuring the performance of space mirrors. Two design optimization examples were provided: one to determine the optimal number of glue pad contacts with reduced constraints, and another to optimize a bipod flexure to support a lightweight mirror with a 500 mm outer diameter, intended for use in a space satellite.

The study analyzed the influence of Von-Mises stress on glue pad performance between the mirror and support under varying temperatures and geometric parameters. The analysis revealed that insufficient attention to thermo-elastic effects could lead to significant distortion and deformation of the mirror. However, through optimization, a better configuration for the number of glue pad contacts was identified, reducing distortion in half of the cases studied. This outcome was further validated through margin of safety analysis, which identified potential failure modes.

In conclusion, finite element analysis has proven to be an invaluable tool for achieving optimal designs for space mirror assemblies. The results of this study contribute to reducing costs and project timelines in space activities, providing a more efficient path toward successful satellite mirror design and manufacturing.

Acknowledgments: The authors would like to thank the Algerian Space Agency, the Centre of satellites Development, and Surrey Space Centre (UK) for their support of this research. Additionally, the author would like to thank M. Diego Angarita-Jaimes for this assistance and advice during the period SSTL, UK know-how transfer technology program.

Conflict of interest: The author declares no conflict of interest.

References

1. Reiss RS. Keynote Address Opto-Mechanical Instrument Design. Optomechanical Systems Engineering. 1987; 0817: 154. doi: 10.1117/12.967421
2. Chin D. Optical Mirror-Mount Design and Philosophy. Applied Optics. 1964; 3(7): 895. doi: 10.1364/ao.3.000895
3. Slocum A. Kinematic couplings: A review of design principles and applications. International Journal of Machine Tools and Manufacture. 2010; 50(4): 310-327. doi: 10.1016/j.ijmachtools.2009.10.006
4. Hale LC, Slocum AH. Optimal design techniques for kinematic couplings. Precision Engineering. 2001; 25(2): 114-127. doi: 10.1016/S0141-6359(00)00066-0
5. Fang S, Hai H, Zhang R, et al. Design of the primary mirror assembly for a space gravitational wave based on the optical path variation model. Applied Optics. 2024; 63(17): 4598. doi: 10.1364/ao.520536
6. Liu S, Hu R, Li Q, et al. Topology optimization-based lightweight primary mirror design of a large-aperture space telescope. Applied Optics. 2014; 53(35): 8318. doi: 10.1364/ao.53.008318
7. Jiang P, Xue C, Wang K, et al. Design and optimization of the tripod flexure for a 2m lightweight mirror for space application. Applied Optics. 2022; 62(1): 217. doi: 10.1364/ao.476783
8. Guo J, Qin T, Han P, et al. Research on the position of the neutral surface of the space lightweight mirror with a two-axis bipod flexible mount. Optics Express. 2024; 32(23): 42126. doi: 10.1364/oe.541310
9. Jiang P, Wang X, Wang K, et al. Lightweight structure and unequal length flexible support design of a 1.3×1.2 m rectangular, horizontally supported mirror. Applied Optics. 2024; 63(27): 7244. doi: 10.1364/ao.531478
10. Tomar S, Meena BR. Design of primary mirror mount for spaceborne EO payload. International conference on small satelittes; 2020.
11. Liu G, Guo L, Wang X, et al. Topology and parametric optimization based lightweight design of a space reflective mirror. Optical Engineering. 2018; 57(07): 1. doi: 10.1117/1.oe.57.7.075101
12. Jiang P, Zhou P. Optimization of a lightweight mirror with reduced sensitivity to the mount location. Applied Optics. 2020; 59(12): 3799. doi: 10.1364/ao.383391
13. Zhang Y, Wang J, Liu J, et al. Accurate modeling of thermal-optical performance for a lightweight SiC mirror. Applied Optics. 2024; 63(20): 5421. doi: 10.1364/ao.529502
14. Chen YC, Huang BK, You ZT, et al. Optimization of lightweight structure and supporting bipod flexure for a space mirror. Applied Optics. 2016; 55(36): 10382. doi: 10.1364/ao.55.010382
15. Dong Z, Zhu J, Liu Z, et al. Structural stability design of an optical mirror mount adjustment mechanism. Applied Optics. 2023; 62(35): 9291. doi: 10.1364/ao.501644
16. Lee J, Rhee HG, Son ES, et al. Optimal design of a coudé mirror assembly for a 1-m class ground telescope. Current Optics and Photonics. 2023; 7(4): 435-442.
17. Liu X, Zhang X, Tian F. Opto-mechanical design of monocrystalline silicon mirror for a reflective imaging optical system. Current optics and Photonics. 2022; 6(3): 236-243.
18. Yoder P, Vukobratovich D. Opto-mechanical systems design, design and analysis of opto-mechanical assemblies, 4th ed. Taylor1&Francis Group; Volume.1, 2015.
19. Yoder P, Vukobratovich D. Opto-mechanical systems design, design and analysis of opto-mechanical assemblies, 4th ed. Taylor1&Francis Group; Volume.2, 2015.
20. Schwertz K, Burge JH. Field guide to optomechanical design and analysis. Society of Photo-optical Instrumentation Engineers (SPIE); 2012.
21. Vukobratovich D, Yoder P. Fundamentals of Optomechanics. CRC Press; 2018. doi: 10.1201/9781351210867
22. Anees A. Handbook of optomechanical engineering. CRS Press; 2017. doi: 10.4324/9781315153247
23. Venzel VI, Dmitriev IYu, Murav'eva ES, et al. Technology for developing a high-aperture four-mirror lens with aspherical mirrors. Journal of Optical Technology. 2023; 90(1): 14. doi: 10.1364/jot.90.000014
24. Kihm H, Lee YW. Optimization and Tolerance Scheme for a Mirror Mount Design Based on Optomechanical Performance. Journal of the Korean Physical Society. 2010; 57(3): 440-445. doi: 10.3938/jkps.57.440

25. Kihm H, Yang HS, Moon IK, et al. Adjustable bipod flexures for mounting mirrors in a space telescope. Applied Optics. 2012; 51(32): 7776. doi: 10.1364/ao.51.007776
26. Shivaprakashb P, Venkateswaran R, Raha B. Design optimization of bipod flexural mount for large size light weighted mirror for space applications. Physics; 2015.
27. Liu B, Wang W, Qu YJ, et al. Design of an adjustable bipod flexure for a large-aperture mirror of a space camera. Applied Optics. 2018; 57(15): 4048. doi: 10.1364/ao.57.004048
28. Huo T, Yu J, Zhao H. Design of a kinematic flexure mount for precision instruments based on stiffness characteristics of flexural pivot. Mechanism and Machine Theory. 2020; 150: 103868. doi: 10.1016/j.mechmachtheory.2020.103868
29. Zhang L, Wang T, Zhang F, et al. Design and optimization of integrated flexure mounts for unloading lateral gravity of a lightweight mirror for space application. Applied Optics. 2021; 60(2): 417. doi: 10.1364/ao.414054
30. Hatheway AE, Vukobratovich D, Yoder PR, Genberg VL. Analysis of adhesive bonds in optics. In: opto mechanical design. SPIE; 1993.
31. Bass M, Van Stryland EW, Wiliams DR, Wolfe WL. Handbook of optics. Fundamentals, technique and design, 2 ed. The optical society of America; 1995.
32. Yoder P. Opto-mechanical systems design, 3rd ed. SPIE Press; 2006.
33. Maamar F, Boudjemai A. Optomechanical optimal design configuration and analysis of glue pad bonds in lens mounting for space application. Advances in Space Research. 2020; 65(10): 2263-2275. doi: 10.1016/j.asr.2020.01.025
34. Yoder PR. Mounting optics in optical instruments. In: Society of photos-optical instrumentation engineers, 2 ed. SPIE Press Bellingham, Washington; 2008.
35. Michels G, Genberg V. SigFit reference manual. Sigmadyne copyright; 2011.